Insight into the description of van der Waals forces for benzene adsorption on transition metal (111) surfaces

Javier Carrasco[1],* Wei Liu[2], Angelos Michaelides[3], and Alexandre Tkatchenko[2†]

[1] *CIC Energigune, Albert Einstein 48, 01510 Miñano, Álava, Spain*

[2] *Fritz-Haber-Institut der Max-Planck-Gesellschaft, Faradayweg 4-6, D-14195, Berlin, Germany*

[3] *Thomas Young Centre, London Centre for Nanotechnology and Department of Chemistry, University College London, London WC1E 6BT, United Kingdom*

Abstract

Exploring the role of van der Waals (vdW) forces on the adsorption of molecules on extended metal surfaces has become possible in recent years thanks to exciting developments in density functional theory (DFT). Among these newly developed vdW-inclusive methods, interatomic vdW approaches that account for the nonlocal screening within the bulk [V. G. Ruiz, W. Liu, E. Zojer, M. Scheffler, and A. Tkatchenko, Phys. Rev. Lett. **108**, 146103 (2012)] and improved nonlocal functionals [J. Klimeš, D. R. Bowler, and A. Michaelides, J. Phys.: Condens. Matter **22**, 022201(2010)] have emerged as promising candidates to account efficiently and accurately for the lack of long-range vdW forces in most popular DFT exchange-correlation functionals. Here we have used these two approaches to compute benzene adsorption on a range of close-packed (111) surfaces upon which it either physisorbs (Cu, Ag, and Au) or chemisorbs (Rh, Pd, Ir, and Pt). We have thoroughly compared the performance between the two classes of vdW-inclusive methods and when available compared the results obtained with experimental data. By examining the computed adsorption energies, equilibrium distances, and binding curves we conclude that both methods allow for an accurate treatment of adsorption at equilibrium adsorbate-substrate distances. To this end, explicit inclusion of electrodynamic screening in the interatomic vdW scheme and optimized exchange functionals in the case of nonlocal vdW density functionals is mandatory. Nevertheless, some discrepancies are found between these two classes of methods at large adsorbate-substrate separations.

I. INTRODUCTION

Van der Waals (vdW) forces are ubiquitous in the binding of atoms and molecules. Although they are relatively weak compared to, for example, covalent and ionic bonding, vdW forces play an important role in fields as diverse as macromolecular biochemistry, supramolecular chemistry, and condensed matter physics.[1–3] Yet despite this importance our current understanding of vdW forces comes mainly from the study of atoms and small molecules in the gas phase, and much less is known about vdW interactions in large aggregates and extended systems of interest in basic and applied science. It is not surprising then that accurately accounting for vdW forces and understanding the role they play in extended systems has become a thriving topic of research in recent years.

From a theoretical viewpoint, density functional theory (DFT) is the method of choice to gain insight into the electronic structure of relatively large systems (typically hundreds of atoms). However the widely used generalized gradient approximation (GGA) functionals, which are generally employed in DFT studies of extended systems, fail to describe non-local vdW forces (as reported, for example, in Ref.[4]). Fortunately, great progress has been made recently in remedying this long-standig problem (see, *e.g.*, Refs. [5–8] and Ref. [9] for a recent review), making it possible to account efficiently and accurately for the long-range vdW energy of solids, extended surfaces, and adsorption processes.[10–12] Weakly interacting atoms and molecules on metal surfaces have become the workhorse systems for understanding how vdW forces influence the interaction of adsorbates with solid substrates in general. Typical examples include benzene, water and noble gases adsorbed on various transition metal surfaces,[11,13–29] C_{60} on Au(111),[30] graphene on Ni(111) and Ir(111),[31–34] self-assembled monolayers of thiolates on Pt(111),[35] pyridine on Cu(110),[36] and isophorone on Pd(111).[37] A common conclusion from these studies is that the inclusion of vdW forces into DFT-GGA calculations often results in a large increase in binding energies and in adsorption distances that are in better agreement with experimental data. Moreover, in some instances vdW forces can also influence qualitatively the adsorption mechanism, allowing for different minima in binding curves,[32,33] promoting chemisorption,[36] tipping the balance between chemisorption and physisorption states,[38] or enabling specific reaction pathways.[37]

In previous papers,[18,39] we showed that when vdW interactions are accurately accounted for, quantitative treatment of both chemisorbed and physisorbed benzene molecules on metal

surfaces becomes possible. In addition, Yildrim *et al.* have recently applied a range of van der Waals density functionals (vdW-DF) to study the binding of benzene on metal surfaces, underscoring this conclusion.[20] However, despite this recent progress, many important questions remain. For example, there are major gaps in our understanding of the general strengths and limitations of the various vdW-corrected methods when applied to these systems. Also very little is known about the performance of these methods at non-equilibrium adsorbate-substrate distances. From the chemical perspective our understanding of the physical nature of the interaction between benzene and metal surfaces is still quite shallow as is our understanding of which metal surfaces can support physisorbed (so-called precursor) states of benzene. In the current follow-on paper we extend our work on these systems aiming precisely to address these important unresolved issues. To this end we have considered two of the most recently developed approaches: the PBE+vdW$^{\mathrm{surf}}$ method[11] and vdW-DF[5] together with some of its offspring.[8,40,41] For comparison we have also included some selected calculations using the Perdew-Burke-Ernzerhof (PBE) exchange-correlation functional[42] and the PBE+vdW scheme.[6]

We have applied these approaches to the adsorption of benzene on the (111) surface of Cu, Ag, Au, Rh, Pd, Ir, and Pt. The benzene-metal system is of interest in basic and applied surface science[43–47] and is an excellent model system to test different vdW-inclusive methods because it has been extensively studied both theoretically[13–18,48–53] and experimentally[17,54–63] in recent years. In particular, we used PBE+vdW$^{\mathrm{surf}}$ and vdW-DF approaches to obtain adsorption energies and equilibrium geometries which we compare with the most recent experimental data available. From the current study we find that both PBE+vdW$^{\mathrm{surf}}$ and certain improved versions of vdW density functionals are capable of reaching quantitative agreement with experimental measurements. In addition, we computed the binding-energy curves of both physisorbed and chemisorbed benzene molecules on all the investigated metal surfaces. In our previous work we found that vdW interactions are important to properly describe a metastable precursor state on Pt and Ir surfaces.[18] Here we also extend this study to the chemisorption of benzene on Rh and Pd, where interestingly we find that such metastable precursor states are not present. This leads us to the suggestion that only sufficiently polarizable metal surfaces are able to give rise to physisorbed precursor states. We also notice that different choices for including relativistic effects lead to some deviations in the binding-energy curves.

This paper is organized as follows. Section II sets out the details of the DFT calculations and approaches considered. Section III reports and discusses computed adsorption energies, equilibrium energies, and binding-energy curves obtained with different vdW-inclusive DFT approaches. Section IV brings a recapitulation and summary of results.

II. THEORETICAL METHODS AND COMPUTATIONAL DETAILS

A. PBE, PBE+vdW, and PBE+vdW^{surf} calculations

We performed DFT calculations using the semi-local PBE exchange-correlation functional[42] and two different vdW-inclusive approaches: the PBE+vdW[6] and the PBE+vdW^{surf} methods[11]. The PBE+vdW method is based on a pairwise atom-atom approximation, whereas the PBE+vdW^{surf} goes beyond this approach and includes electrodynamic screening of vdW interactions by combining intermolecular vdW interactions with the Lifshitz-Zaremba-Kohn theory[64] for the dielectric screening within the metal surface. PBE, PBE+vdW, and PBE+vdW^{surf} calculations were carried out using the numeric atom-centered basis set all-electron code FHI-aims[65,66] applying an atomic zeroth-order regular approximation (ZORA) for treating relativistic effects, in order to consistently compare with pseudopotential results. We used "tight" settings, including the "tier2" standard basis set in the FHI-aims code for H and C atoms, and the "tier1" basis set for transition metal atoms. We set the following thresholds for the convergence criteria: 0.01 AA^{-1} for the final forces in all structural relaxations, 10^{-5} electrons for the electron density, and 10^{-4} eV for the total energy of the system. A Monkhorst-Pack[67] grid with 18×18×1 **k**-point sampling per (1×1) unit cell was used for slab calculations. We applied a dipole correction along the direction perpendicular to the metal surface.[68,69] These computational settings guarantee a convergence in the adsorption energies and equilibrium distances better than 0.01 eV and 0.01 Å, respectively (Table I).

The unreconstructed close-packed (111) surfaces were modeled by periodic (3×3) unit cells, containing 6 atomic layers separated by at least 20 Å of vacuum, which ensures that the interaction between the adsorbed benzene molecule and the periodic images of the metal slab is negligible. The benzene molecule and the uppermost two metal layers were allowed to relax during geometry relaxation. The four bottom metal layers were fixed at their bulk-

truncated positions using the lattice constants of the bulk metals from each method (Table II). Although the PBE+vdW$^{\rm surf}$ method slightly overestimates the interaction between metallic electrons in the bulk as discussed in Ref. [39], the performance of the PBE+vdW$^{\rm surf}$ method for lattice constants is very similar to PBE.

B. Non-local density functional calculations

We considered the following non-local exchange-correlation functionals: the vdW-DF of Dion *et al.*,[5] the vdW-DF2 of Murray *et al.*[40] and Lee *et al.*;[41] and three optimized versions of the vdW-DF.[8,70] The vdW-DF2 functional aims to improve the binding description around energy minima in relation to vdW-DF by changing both the exchange and non-local correlation components. In the optimized versions of the vdW-DF, its original GGA functional has been replaced by an optimized PBE (optPBE), optimized Becke88 (optB88), or optimized Becke86b (optB86b) to improve the accuracy of both vdW-DF and vdW-DF2 schemes. These three optimized functionals are referred to as optPBE-vdW, optB88-vdW, and optB86b-vdW herein, respectively.

All vdW density functional calculations were carried out self-consistently within the VASP code[71,72] as implemented by Klimeš *et al.*[70] using the algorithm of Román-Pérez and Soler.[73] In all cases the core electrons were replaced by PBE-based projector augmented wave (PAW) potentials.[74] We treated explicitly the H ($1s$), C ($2s$, $2p$), Cu ($3p$, $3d$, $4s$), Ag ($4d$, $5s$), Au ($5d$, $6s$), Rh ($4d$, $5s$), Pd ($4d$, $5s$), Ir ($5d$, $6s$), and Pt ($5d$, $6s$) electrons as valence electrons and their wavefunctions were expanded in plane-waves with a cut-off energy of 500 eV. A Monkhorst-Pack[67] grid with 12×12×1 **k**-point sampling per (1×1) unit cell was used. We again applied a dipole correction along the direction perpendicular to the metal surface[68,69] and geometry optimizations were performed with a residual force threshold of 0.03 eVÅ^{-1}.

Using the lattice constants of the bulk metal from each functional (Table II), we built up 6-layer slabs with a (3×3) unit cells and separated by at least 12 Å (18 Å when computing binding curves). The metal atoms in the three bottom layers were fixed at their bulk-truncated positions during structure relaxation. The metal lattice constants computed here (Table II) are in good agreement (differences are less than 0.020 Å) with the values reported in the literature using the same vdW functionals.[20,70] In general, vdW-DF and vdW-DF2 tend to overestimate all values with respect to experimental data. The largest errors are

0.191 Å (0.268 Å) for vdW-DF (vdW-DF2) in the case of Ag (Au). This behavior can be traced back to the fact that these two functionals are too repulsive at short interatomic separations,[40] which is important for the correct description of lattice constants. The use of less repulsive exchange functionals at short separations reduces the errors significantly,[70] giving better agreement with the reference experimental data for the transition metals considered here. Specifically, the largest differences with experimental values are reduced to 0.113 Å, 0.093 Å, and 0.052 Å by using optPBE-vdW, optB88-vdW, and optB86b-vdW, respectively. Overall the performance of these functionals, and in particular optB88-vdW and optB86b-vdW, for transition metal lattice constants is as good or better than PBE and PBE+vdW$^{\rm surf}$.

C. Adsorption energies and geometries

The adsorption energies of benzene on the investigated (111) metal surfaces were computed as follow:

$$E_{\rm ads} = E_{\rm Bz-M} - E_{\rm M} - E_{\rm Bz}, \tag{1}$$

where $E_{\rm Bz-M}$ is the total energy of the adsorbed benzene molecule, $E_{\rm M}$ is the total energy of the relaxed bare metal slab, and $E_{\rm Bz}$ is the total energy of a relaxed gas-phase benzene molecule in the same unit cell used to compute the total system, but without the metal slab. In addition, we considered the non-local correlation part, $E^{\rm nlc}$, of the total exchange-correlation energy to compute the corresponding non-local correlation contribution to the adsorption energy, $E^{\rm nlc}_{\rm ads}$, as follow:

$$E^{\rm nlc}_{\rm ads} = E^{\rm nlc}_{\rm Bz-M} - E^{\rm nlc}_{\rm M} - E^{\rm nlc}_{\rm Bz}. \tag{2}$$

where the subindexes Bz-M, M, and Bz stand for the adsorbed benzene molecule, the relaxed bare metal slab, and a relaxed gas-pahse benzene molecule.

Equilibrium geometries were characterized by considering two average perpendicular heights ($d_{\rm CM}$ and $d_{\rm HM}$ for C–metal and H–metal distances, respectively), which are referenced to the average z positions of the relaxed topmost metal atoms.

We computed the adsorption energy of the system as a function of the perpendicular height, d, between the carbon backbone of the benzene molecule and the metal surface. We

evaluated d relative to the position of the topmost metal layer of the bare surface. Notice that due to the optimization constraints imposed on the carbon backbone (the z coordinate of the 6 carbon atoms was fixed) of the benzene molecule, the location of equilibrium minima in the computed binding curves may slightly differ in some cases from the fully relaxed calculations described above.

D. Level of convergence

The computational settings described in Sections II A and II B guarantee a tight convergence in adsorption energies and equilibrium distances as assessed by an extensive series of convergence tests performed for the adsorption of benzene on Au and Pt. Table I summarizes the computed $E_{\rm ads}$, $d_{\rm CM}$, and $d_{\rm HM}$ values using PBE+vdW$^{\rm surf}$ and optB88-vdW as a function of the basis set size, **k**-point mesh size, vacuum between slabs, total number of layers in the slab, and number of relaxed layers in the slab. In particular, PBE+vdW$^{\rm surf}$ (optB88-vdW) benzene adsorption energies are better than 0.02 eV (0.02 eV) on Au and better than 0.04 eV (0.01 eV) on Pt. Equilibrium distances are in all cases better than 0.01 Å.

Aiming at comparison between FHI-aims and VASP results, we computed the adsorption energy of benzene on Au and Pt using PBE with these two codes. The FHI-aims (VASP) results for Au and Pt are -0.08 eV(-0.03 eV) and -1.00 eV (-1.02 eV), respectively. These differences are very small and mainly reflect differences in the underlying basis sets: all-electron plus atomic ZORA treatment of relativistic effects (FHI-aims) and plane-waves plus PAW potentials (VASP).

III. RESULTS AND DISCUSSION

A. Adsorption energies and equilibrium geometries

Benzene adsorption is weaker on (111) coinage metal surfaces (Cu, Ag, and Au) than on transition metals with unfilled d bands (Rh, Pd, Ir, and Pt).[45] For example, the experimental adsorption energy of benzene on Au is 0.73–0.87 eV,[59] whilst the interaction with Pt is stronger, 1.57–1.91 eV.[60] This is a direct consequence of the position of the d-band center, which is substantially below the Fermi level in the case of coinage metals. A weak

benzene-metal interaction (physisorption) implies a flat potential energy surface (PES) and, therefore, benzene molecules can easily diffuse over the surface, as it has been found by scanning tunneling microscopy (STM) experiments on Cu(111) and Au(111) terraces at low temperatures.[58,61,62] These observations have been supported recently by DFT calculations by some of us,[18,39] where the predicted energy difference among eight high-symmetry adsorption sites of benzene on Au(111)[75] was only 0.04 eV using PBE+vdW$^{\rm surf}$. Among the most preferable adsorption sites was a bridge configuration with an angle of 30° between the C–C and Au–Au bonds (referred to as bri30° herein). This adsorption geometry is shown in Fig. 1. The preference for the bri30° site in the case of Pt is also supported by low-energy electron diffraction (LEED)[55] and STM[56] experiments.

In our previous work[39] we showed that the bri30° site is preferred for chemisorption (on Rh, Pd, Ir, and Pt) of benzene when considering PBE, PBE+vdW, and PBE+vdW$^{\rm surf}$. In the case of physisorbed systems (on Cu, Ag, and Au) the relative stability among most of the eight high-symmetry adsorption sites is very small (less than 0.02 eV), but all three methods predict the bri30° site to be in the group of the most favorable adsorption sites. In the following we focus on the bri30° site to examine the performance of a range of different methods: PBE+vdW, PBE+vdW$^{\rm surf}$, vdW-DF, vdW-DF2, optPBE-vdW, optB88-vdW, optB86b-vdW, and for reference PBE. The computed adsorption energies and equilibrium geometries of benzene on Cu, Ag, Au, Rh, Pd, Ir, and Pt are summarized in Tables III and IV, respectively. A key observation is that PBE yields negligible adsorption energies of benzene on coinage metal surfaces and largely underbinds on Rh, Pd, Ir, and Pt. For example, the PBE adsorption energy on Pt is *ca.* 0.9 eV lower than the experimental value (Table III). The adsorption energies are systematically improved in all cases upon inclusion of vdW forces by means of the PBE+vdW method. Further refinement of these calculated values is achieved when explicitly accounting for the dielectric screening by electrons inside the bulk metal through the PBE+vdW$^{\rm surf}$ method, which takes into account the reduction of both the C_6 coefficient and vdW radius of the metal atoms.[39] In particular, the effect of screening decreases the adsorption energies on coinage metals and Rh by 0.1–0.2 eV, whereas the interaction is enhanced in the case of Pd, Ir, and Pt. It is notable that the inclusion of the collective response effects reduces both vdW C_6 coefficients and vdW radii, leading to opposite effects in the vdW energy and resulting in non-trivial behaviour for different metals.[39]

Moving to the results from the vdW density functionals, we find that the agreement with the available experimental data strongly depends on the particular choice of the underlying exchange functional. Consistent with previous studies for various adsorption systems, the vdW-DF and vdW-DF2 functionals yield even smaller adsorption energies than PBE.[5,8,18,26,41,76–78] Nevertheless, switching to improved underlying exchange functionals (optPBE, optB88, and optB86b) consistently provides larger adsorption energies than PBE and quantitative agreement (especially for optB88-vdW) with PBE+vdW$^{\mathrm{surf}}$ and available experimental data. Similar findings have recently been reported by Yildirim *et al.*[20] It is important to stress that for the S22 database all the optimized density functionals considered here essentially yield similar results.[8] In contrast, for benzene adsorption on transition metals, especially in the case of strongly bound systems, the situation is more complex. In particular, adsorption energies differ up to 0.6-0.7 eV on the four reactive metals when using optPBE-vdW, optB88-vdW, or optB86b-vdW (Table III). Further analysis shows that adsorption energy enhancements to the benzene-metal bonding are largely due to non-local correlation, $E_{\mathrm{ads}}^{\mathrm{nlc}}$ (Eq. 2), which is the principal attractive contribution to the total adsorption energy at the equilibrium geometry (Fig. 2). Indeed the magnitude of $E_{\mathrm{ads}}^{\mathrm{nlc}}$ on all surfaces is greater than the total adsorption energy. On the most reactive metals (Rh, Pd, Ir, and Pt) the larger covalent character of the bonding (chemisorption) is reflected by larger $E_{\mathrm{ads}}^{\mathrm{nlc}}$ than on coinage metals. We notice that vdW-DF2 systematically yields the lowest $E_{\mathrm{ads}}^{\mathrm{nlc}}$ compared to the other functionals (especially in the case of the more reactive metals), which explains why the smallest adsorption energies are found for this functional (Table III).

The three optimized exchange functionals (optPBE, optB88, and optB86b) show similar non-local correlation contributions upon any given metal surface. Specifically, the differences between $E_{\mathrm{ads}}^{\mathrm{nlc}}$ values computed using these three exchange functionals for a given system are less than 0.18 eV on coinage metals and less than 0.10 eV on reactive metals (Fig. 2). This behavior explains why on the coinage metal series the adsorption energies computed with optPBE-vdW, optB88-vdW, or optB86b-vdW are very similar: the energy differences are less than 0.10 eV (Table III). On the other hand, on reactive metals the computed adsorption energies show much larger energy differences despite $E_{\mathrm{ads}}^{\mathrm{nlc}}$ being similar. This result highlights the fact that on such systems the benzene-metal bonding is dominated by covalency. In particular, we found that the energy difference between $E_{\mathrm{ads}}^{\mathrm{nlc}}$ and E_{ads} provides a useful descriptor to rationalize the behavior of each functional when describing the benzene-metal

bonding on chemisorbed systems. To this end, we define the ratio of attractive non-local correlation lost after adding all the remaining contributions to the bonding, $\chi_{\rm ads}^{\rm nlc}$, as

$$\chi_{\rm ads}^{\rm nlc} = \frac{E_{\rm ads}^{\rm nlc} - E_{\rm ads}}{E_{\rm ads}^{\rm nlc}}. \quad (3)$$

Essentially, $\chi_{\rm ads}^{\rm nlc}$ indirectly quantifies how repulsive a given functional is. This is important because the position of the repulsive Pauli wall is the main aspect that ultimately controls the performance of a vdW density functional at short distances (equilibrium distances in chemisorption). As shown in Fig. 3, we find a linear correlation between $E_{\rm ads}$ and $\chi_{\rm ads}^{\rm nlc}$ for all chemisorbed systems. The adsorption energy decreases when increasing $\chi_{\rm ads}^{\rm nlc}$, i.e. a more repulsive exchange functional yields lower adsorption energies. Interestingly, vdW-DF2 also fits well on this linear regression, even though it has a different underlying correlation term than the rest of density functionals. From Fig. 3 it is clear that vdW-DF2 is the most repulsive functional followed by vdW-DF, optPBE-vdW, optB88-vdW, and optB86b-vdW. All three optimized exchange functionals show $\chi_{\rm ads}^{\rm nlc}$ values below 0.5, whereas vdW-DF and vdW-DF2 lead to larger values. Considering that optB88-vdW shows the best agreement with available experimental data, Fig. 3 suggests that density functionals with $\chi_{\rm ads}^{\rm nlc}$ values ranging between 0.2 and 0.4 are particularly suitable to achieve a good description of the adsorption energy and equilibrium geometry for these systems. Therefore, $\chi_{\rm ads}^{\rm nlc}$ of adsorbed benzene on late transition metals could be a good descriptor to assess the accuracy of a given vdW-DF type density functional for other adsorbates on late transition metals. Actually similar conclusions are also found for water adsorption on transition metals.[26] Nevertheless, further work is required to see whether this is a general trend.

Another key observation is that on Rh, Pd, Ir, and Pt the benzene loses its gas-phase planar configuration upon adsorption with hydrogen atoms tilting upward after relaxation and resulting in two averaged perpendicular heights: a relatively short C–metal ($d_{\rm CM}$) and a relatively long H–metal ($d_{\rm HM}$) distances as shown in Fig. 1b and Table IV. In contrast, on coinage metal surfaces the benzene molecule adsorbs almost flat (Fig. 1a). This qualitative difference in the equilibrium geometry between chemisorbed and physisorbed systems is captured by all the methods considered, including PBE. From a quantitative viewpoint, the performance of each method is less homogeneous though. Focusing first on physisorbed systems, including the vdW energy through the PBE+vdW method has a dramatic impact

on d_{CM}, which is shortened by 0.41–0.70 Å with respect to PBE distances (Table IV). Collective screening effects bring the benzene molecule even closer to the the surface by 0.18–0.25 Å (cf. PBE+vdW and PBE+vdW$^{\mathrm{surf}}$ values in Table IV). In this respect, vdW-DF predicts very large d_{CM}, even larger in most cases than the PBE values. Although vdW-DF2 substantially improves the vdW-DF equilibrium geometries, the differences with PBE+vdW$^{\mathrm{surf}}$ are still large, 0.24–0.56 Å (Table IV). The other density functionals predict equilibrium geometries close to the PBE+vdW$^{\mathrm{surf}}$ values, in particular optB88-vdW and optB86b-vdW present Δd_{CM} equal to 0.16–0.29 Å and 0.07–0.33 Å, respectively (Table IV). Considering now the chemisorbed case, relatively similar equilibrium distances are obtained with all eight methods (Table IV). This result indicates that in such strongly bound systems the chemical bond largely controls the adsorption height.

All investigated methods predict very similar internal structures of the benzene molecule. In particular, the C–C distances (l_{CC1} and l_{CC2}) are almost identical no matter whether PBE, PBE+vdW, PBE+vdW$^{\mathrm{surf}}$, vdW-DF, vdW-DF2, optPBE-vdW, optB88-vdW, or optB86b-vdW is used (Table IV). This indicates that the chemical bonds within the benzene molecule are similarly well described by all the methods considered.

B. Binding-energy curves

We discuss now the role of vdW forces on the the binding-energy curves and their dependence on the specific method used. First we calculated the PBE, PBE+vdW$^{\mathrm{surf}}$, vdW-DF, vdW-DF2, and optB88-vdW binding curves of a benzene molecule on Au and Pt as representatives of physisorption and chemisorption, respectively (Fig. 4). Each point in these graphs was obtained by keeping fixed the carbon backbone height d from the surface as described in Sec. II C. On the two metal surfaces, of the methods considered, PBE predicts the weakest interaction at long range (for $d > 6.0$ Å), pointing out its lack of non-local vdW forces. All the other methods recover to some extent the vdW-attraction at long range. Important quantitative differences among the vdW-inclusive approaches considered remain though. For example, vdW-DF and vdW-DF2 present a general tendency toward larger binding energies than PBE on Au and the physisorption region of Pt. The situation is significantly worse for the chemisorption region on Pt, where the two functionals predict the chemisorbed well to be shallower than the PBE minimum. Indeed vdW-DF2 predicts the chemisorbed well to

be even shallower than the precursor physisorption-well minimum. This situation is much improved when considering optB88-vdW for both Au and Pt, optB88-vdW predicts a well depth and potential minimum location that lie close to the experimental data. Similarly, PBE+vdW$^{\rm surf}$ shows good performance. Both optB88-vdW and PBE+vdW$^{\rm surf}$ give similar estimates for equilibrium distances and binding energies, especially in the case of Au. In addition, the precursor physisorption state for Pt is only clearly well defined when using vdW-DF and vdW-DF2, whilst PBE+vdW$^{\rm surf}$ and optB88-vdW hardly predict a true minimum, but a barrier-less transition between the chemisorbed and physisorbed states. We note in passing that the PBE+vdW$^{\rm surf}$ calculations in this paper employ atomic ZORA for the treatment of scalar relativistic effects to enable one-to-one comparison with pseudopotential calculations. Our previous work with scaled ZORA,[18,38,39] which explicitly includes scalar-relativistic effects in the orbital energies of the full system, yielded better agreement with experiments and lead to the appearance of a shallow physisorption precursor state for benzene on Pt.

We notice the existence of a very shallow metastable precursor physisorption state on Ir(111) when considering optB88-vdW (Fig. 5), where the barrier to adsorption predicted by PBE essentially vanishes. Nevertheless, on Rh and Pd there exists a perturbation to the binding curve that suggests an underlying small physisorption-like interaction between 3.0-3.5 Å, but neither PBE+vdW$^{\rm surf}$ nor optB88-vdW are able to resolve a clear minimum. Since the stability of the physisorption state is determined mainly by vdW interactions,[37] this result suggests that the larger polarizability of the $5d$ (Ir and Pt) compared to the $4d$ (Rh and Pd) metals for the same number of valence electrons is responsible for this behavior. In particular, the C_6 coefficients computed with PBE+vdW$^{\rm surf}$ are C_6^{Ir}=98 hartree $\cdot$ bohr^6 to be compared with C_6^{Rh}=84 hartree $\cdot$ bohr^6 and C_6^{Pt}=120 hartree $\cdot$ bohr^6 to be compared with C_6^{Pd}=102 hartree $\cdot$ bohr^6.

Another important difference between the binding-energy curves in Fig. 4 is the description of the interaction at large distances from the surface, where the vdW attraction dominates. In this case different methods give rise to rather different asymptotic decays. For example, when comparing vdW-DF and vdW-DF2, both binding curves lie very close to each other in the Pauli-repulsion region at short binding distances on Au and the physisorption region on Pt, but vdW-DF2 decays faster in the vdW-attraction region at separations larger than 4 Å. In order to quantify these differences we have considered the traditional

picture of physisorption where the long-ranged vdW attractive potential goes approximately like (see, e.g., Refs. [64,79,80])

$$V_{\mathrm{vdW}}(d) = C_3(d - d_0)^{-3}. \tag{4}$$

Here d is the distance of the adsorbate normal to the uppermost surface layer of atom cores in the solid. Usually one can fit the adsorption energy as a function of d by optimizing this expression[81,82] and estimating the strength of the asymptotic vdW attraction, C_3, and the surface image reference-plane, d_0. Often d_0 is very close to one half of the metal interlayer separation ($\sim$1.2 Å for Au and Pt). Following this procedure we have fitted the data shown in Fig. 4 for PBE+vdW$^{\mathrm{surf}}$ and d values larger than 9 Å. Only the vdW contribution to the adsorption energy in this region was taken into account for the fitting. Table V shows the corresponding C_3 coefficients for Au and Pt. We note that the PBE+vdW$^{\mathrm{surf}}$ energy expression is explicitly constructed to reproduce the *exact* C_3 coefficient by employing the experimental dielectric function and accurate polarizabilities for atoms in molecules. Following a similar procedure we fitted the C_3 coefficients for the vdW-DF type density functionals. In this case we considered the non-local correlation contribution to the adsorption energy (Eq. 2) and we fixed d_0 to the values obtained with PBE-vdW$^{\mathrm{surf}}$ (1.06 Å and 1.03 Å for Au and Pt, respectively). This procedure ensures a proper comparison between the two types of vdW-inclusive methods. As shown in Table V, the C_3 coefficients depend on the method. The vdW-DF2 shows the weakest vdW interaction at this long distance range, yielding C_3 coefficients nearly two times smaller than the rest of methods. This is consistent with the fact that vdW-DF2 heavily underestimate the C_6 coefficients of molecules.[83] On the other hand vdW-DF and optB88-vdW (both sharing the same non-local correlation energy expression by construction) yield C_3 coefficients in good agreement with PBE+vdW$^{\mathrm{surf}}$. We note that such good agreement might be partially accidental, since the vdW-DF correlation energy yields errors of $\sim$20% in the intermolecular C_6 coefficients.[83] However, the agreement in C_3 coefficients between PBE+vdW$^{\mathrm{surf}}$ and vdW-DF (optB88-vdW) further explains the good performance of these methods found for the equilibrium properties of benzene adsorbed on transition metal surfaces.

IV. CONCLUSIONS

We have investigated the performance of a series of vdW-inclusive DFT schemes (PBE+vdW, PBE+vdW$^{\rm surf}$, vdW-DF, vdW-DF2, optPBE-vdW, optB88-vdW, and optB86b-vdW) to compute the adsorption of benzene molecules on transition metal (111) surfaces. Our calculations have demonstrated that an accurate treatment of vdW dispersion interactions is essential to properly account for adsorption energies and equilibrium distances not only in weakly bound systems (Cu, Ag, and Au), but also in strongly bound ones (Rh, Pd, Ir, and Pt). In particular, the performance of PBE+vdW$^{\rm surf}$ and optB88-vdW for predicting adsorption energies and equilibrium geometries are similar and both methods are in agreement with available experimental data.

The performance of the different density functionals analyzed is sensitive to their underlying exchange functional. We put forward that only optimized exchange functionals (optPBE, optB88, and optB86b) are capable of providing reliable results. In this regard, a proper description of the short-ranged Pauli repulsion is critical to accurately describe the investigated chemisorbed systems. We found a convenient descriptor to assess the magnitude of such short-ranged repulsion given a particular vdW-DF type density functional, namely, the energy difference ratio between the total adsorption energy and its non-local correlation contribution, $\chi_{\rm ads}^{\rm nlc}$ (Eq. 3). A large $\chi_{\rm ads}^{\rm nlc}$ implies a more repulsive density functional. We found that the poor performance of vdW-DF and vdW-DF2 can be tracked back to too large $\chi_{\rm ads}^{\rm nlc}$ values, whereas optimized exchange functionals (optPBE, optB88, and optB86b) are much less repulsive, presenting smaller $\chi_{\rm ads}^{\rm nlc}$ values and superior accuracy. In particular, computed adsorption energies show a linear dependence with respect to $\chi_{\rm ads}^{\rm nlc}$ and, therefore, this descriptor could be valuable for further exchange-correlation functional development.

In addition, optB88-vdW predicted a very shallow metastable precursor physisorption state for Ir and Pt. For Rh, and Pd, the metastable state essentially vanished using either PBE+vdW$^{\rm surf}$ or optB88-vdW. Both the polarizability of molecules and substrates are key factors in the appearance of precursor states.[38] Therefore, these results can be explained by the lower polarizability of Rh versus Ir and Pd versus Pt.

Overall, our findings for benzene adsorbed on transition metals suggest that recent developments in vdW-inclusive methods have now reached a sufficient state of maturity that vdW interactions and many-body screening effects can be accounted for at equilibrium

distances for the specific adsorption systems considered. Interestingly, PBE+vdW^{surf} and optB88-vdW, which are two fundamentally different approaches, are both able to achieve nearly equivalent quantitative agreement in adsorption energies and equilibrium distances. Nonetheless some discrepancies between the approaches arise at large adsorbate-substrate distances. Resolving these discrepancies will probably require the application of more sophisticated methods. In general, comparison of methods on these and other adsorption systems along with more accurate experimental measurements (both in terms of structure and energetics) of benzene adsorption on well-defined metal surfaces remain highly desirable.

ACKNOWLEDGMENTS

We are grateful for support from the FP7 Marie Curie Actions of the European Commission, via the Initial Training Network SMALL (MCITN-238804) and the Career Integration Grant (FP7-PEOPLE-2011-CIG `NanoWGS`). J.C. is a Ramón y Cajal fellow and Newton Alumnus supported by the Spanish Government and The Royal Society. W.L. was funded by a fellowship from the Alexander von Humboldt Foundation. A.M. is supported by the ERC (ERC Starting Grant `QUANTUMCRASS`) and by The Royal Society through a Wolfson Research Merit Award. A.T. acknowledges support from the European Research Council (ERC Starting Grant `VDW-CMAT`). We are grateful for computer time to the London Centre for Nanotechnology, the Barcelona Supercomputing Center, and the UK's national high performance computing service HECToR (from which access was obtained via the UK's Material Chemistry Consortium, EP/F067496).

---

* Electronic address: jcarrasco@cicenergigune.com

† Electronic address: tkatchenko@fhi-berlin.mpg.de

[1] A. J. Stone, *The Theory of Intermolecular Forces* (Oxford University Press, 1996).

[2] V. A. Parsegian, *Van der Waals forces: A Handbook for Boilogists, Chemists, Engineers and Physicists* (Cambridge University Press, 2005).

[3] R. H. French, V. A. Parsegian, R. Podgornik, R. F. Rajter, A. Jagota, J. Luo, D. Asthagiri, M. K. Chaudhury, Y.-m. Chiang, S. Granick, et al., Rev. Mod. Phys. **82**, 1887 (2010).

[4] K. Lee, A. K. Kelkkanen, K. Berland, S. Andersson, D. C. Langreth, E. Schröder, P. Hyldgaard, and B. I. Lundqvist, Phys. Rev. B **84**, 193408 (2011).

[5] M. Dion, H. Rydberg, E. Schröder, D. C. Langreth, and B. I. Lundqvist, Phys. Rev. Lett. **92**, 246401 (2004).

[6] A. Tkatchenko and M. Scheffler, Phys. Rev. Lett. **102**, 073005 (2009).

[7] S. Grimme, J. Antony, S. Ehrlich, and H. Krieg, J. Chem. Phys. **132**, 154104 (2010).

[8] J. Klimeš, D. R. Bowler, and A. Michaelides, J. Phys.: Condens. Matter **22**, 022201 (2010).

[9] J. Klimeš and A. Michaelides, J. Chem. Phys. **137**, 120901 (2012).

[10] A. Tkatchenko, L. Romaner, O. T. Hofmann, E. Zojer, C. Ambrosch-Draxl, and M. Scheffler, MRS Bulletin **35**, 435 (2010).

[11] V. G. Ruiz, W. Liu, E. Zojer, M. Scheffler, and A. Tkatchenko, Phys. Rev. Lett. **108**, 146103 (2012).

[12] J. Carrasco, B. Santra, J. Klimeš, and A. Michaelides, Phys. Rev. Lett. **106**, 026101 (2011).

[13] A. K. Kelkkanen, B. I. Lundqvist, and J. K. Nørskov, Phys. Rev. B **83**, 113401 (2011).

[14] M. Vanin, J. J. Mortensen, A. K. Kelkkanen, J. M. Garcia-Lastra, K. S. Thygesen, and K. W. Jacobsen, Phys. Rev. B **81**, 081408 (2010).

[15] K. Toyoda, I. Hamada, K. Lee, S. Yanagisawa, and Y. Morikawa, J. Chem. Phys. **132**, 134703 (2010).

[16] J. Wellendorff, A. Kelkkanen, J. J. Mortensen, B. I. Lundqvist, and T. Bligaard, Top. Catal **53**, 378 (2010).

[17] E. Abad, Y. J. Dappe, J. I. Martínez, F. Flores, and J. Ortega, J. Chem. Phys. **134**, 044701 (2011).

[18] W. Liu, J. Carrasco, B. Santra, A. Michaelides, M. Scheffler, and A. Tkatchenko, Phys. Rev. B **86**, 245405 (2012).

[19] K. Lee, K. Berland, M. Yoon, S. Andersson, E. Schröder, P. Hyldgaard, and B. I. Lundqvist, J. Phys.: Condens. Matter **24**, 424213 (2012).

[20] H. Yildirim, T. Greber, and A. Kara, J. Phys. Chem. C **117**, 20572 (2013).

[21] I. Hamada, K. Lee, and Y. Morikawa, Phys. Rev. B **81**, 115452 (2010).

[22] T. Kumagai, H. Okuyama, S. Hatta, T. Aruga, and I. Hamada, J. Chem. Phys. **134**, 024703 (2011).

[23] A. Poissier, S. Ganeshan, and M. V. Fernández-Serra, Phys. Chem. Chem. Phys. **13**, 3375

(2011).

[24] K. Tonigold and A. Gross, J. Comp. Chem. **33**, 695 (2012).

[25] R. Nadler and J. F. Sanz, J. Chem. Phys. **137**, 114709 (2012).

[26] J. Carrasco, J. Klimeš, and A. Michaelides, J. Chem. Phys. **138**, 024708 (2013).

[27] J. L. F. Da Silva, C. Stampfl, and M. Scheffler, Phys. Rev. Lett. **90**, 066104 (2003).

[28] D. L. Chen, W. A. Al-Saidi, and J. K. Johnson, Phys. Rev. B **84**, 241405 (2011).

[29] P. L. Silvestrelli, A. Ambrosetti, S. Grubisic, and F. Ancilotto, Phys. Rev. B **85**, 165405 (2012).

[30] I. Hamada and M. Tsukada, Phys. Rev. B **83**, 245437 (2011).

[31] C. Busse, P. Lazic, R. Djemour, J. Coraux, T. Gerber, N. Atodiresei, V. Caciuc, R. Brako, A. T. N'Diaye, S. Blugel, et al., Phys. Rev. Lett. **107**, 036101 (2011).

[32] F. Mittendorfer, A. Garhofer, J. Redinger, J. Klimeš, J. Harl, and G. Kresse, Phys. Rev. B **84**, 201401 (2011).

[33] X. Li, J. Feng, E. Wang, S. Meng, J. Klimeš, and A. Michaelides, Phys. Rev. B **85**, 085425 (2012).

[34] S. M. Kozlov, F. Viñes, and A. Görling, J. Phys. Chem. C **116**, 7360 (2012).

[35] M. A. F. Addato, A. A. Rubert, G. A. Benítez, M. H. Fonticelli, J. Carrasco, P. Carro, and R. Salvarezza, J. Phys. Chem. C **115**, 17788 (2012).

[36] N. Atodiresei, V. Caciuc, P. Lazić, and S. Blügel, Phys. Rev. Lett. **102**, 136809 (2009).

[37] W. Liu, A. Savara, X. Ren, W. Ludwig, K.-H. Dostert, S. Schauermann, A. Tkatchenko, H.-J. Freund, and M. Scheffler, J. Phys. Chem. Lett. **3**, 582 (2012).

[38] W. Liu, S. N. Filimonov, J. Carrasco, and A. Tkatchenko, Nature Comms. **4**, 2569 (2013).

[39] W. Liu, V. G. Ruiz, G.-X. Zhang, B. Santra, X. Ren, M. Scheffler, and A. Tkatchenko, New J. Phys. **15**, 053043 (2013).

[40] E. D. Murray, K. Lee, and D. C. Langreth, J. Chem. Theory Comput. **5**, 2754 (2009).

[41] K. Lee, E. D. Murray, L. Kong, B. I. Lundqvist, and D. C. Langreth, Phys. Rev. B **82**, 081101 (2010).

[42] J. Perdew, K. Burke, and M. Ernzerhof, Phys. Rev. Lett. **77**, 3865 (1996).

[43] F. S. Tautz, Prog. Surf. Sci. **82**, 479 (2007).

[44] P. Gomez-Romero, Adv. Mater. **13**, 163 (2001).

[45] S. J. Jenkins, Proc. R. Soc. A **465**, 2949 (2009).

[46] L. Kronik and N. Koch, MRS Bull. **35**, 417 (2010).

[47] Y. P. Tan, S. Khatua, S. J. Jenkins, J. Q. Yu, J. B. Spencer, and D. A. King, Surf. Sci. **589**, 173 (2005).

[48] P. Sautet and C. Joachim, Chem. Phys. Lett. **185**, 23 (1991).

[49] P. Sautet and M. Bocquet, Surf. Sci. **304**, L445 (1994).

[50] P. Sautet and M. Bocquet, Phys. Rev. B **53**, 4910 (1996).

[51] C. Morin, D. Simon, and P. Sautet, J. Phys. Chem. B **107**, 2995 (2003).

[52] C. Morin, D. Simon, and P. Sautet, J. Phys. Chem. B **108**, 5653 (2004).

[53] C. Morin, D. Simon, and P. Sautet, Surf. Sci. **600**, 1339 (2006).

[54] X. Zhou, M. Castro, and J. White, Surf. Sci. **238**, 215 (1990).

[55] A. Wander, G. Held, R. Q. Hwang, G. S. Blackman, M. L. Xu, P. de Andres, M. A. Van Hove, and G. A. Somorjai, Surf. Sci. **249**, 21 (1991).

[56] P. S. Weiss and D. M. Eigler, Phys. Rev. Lett. **71**, 3139 (1993).

[57] M. Xi, M. Yang, S. Jo, B. Bent, and P. Stevens, J. Chem. Phys. **101**, 9122 (1994).

[58] S. Stranick, M. Kamna, and P. Weiss, Surf. Sci. **338**, 41 (1995).

[59] D. Syomin, J. Kim, B. E. Koel, and G. B. Ellison, J. Phys. Chem. B **105**, 8387 (2001).

[60] H. Ihm, H. M. Ajo, J. M. Gottfried, P. Bera, and C. T. Campbell, J. Phys. Chem. B **108**, 14627 (2004).

[61] B. A. Mantooth, E. C. H. Sykes, P. Han, A. M. Moore, Z. J. Donhauser, V. H. Crespi, and P. S. Weiss, J. Phys. Chem. C **111**, 6167 (2007).

[62] E. Abad, J. Ortega, Y. J. Dappe, and F. Flores, Appl. Phys. A **95**, 119 (2009).

[63] K. Toyoda, Y. Nakano, I. Hamada, K. Lee, S. Yanagisawa, and Y. Morikawa, Surf. Sci. **603**, 2912 (2009).

[64] E. Zaremba and W. Kohn, Phys. Rev. B **13**, 2270 (1976).

[65] V. Blum, R. Gehrke, F. Hanke, P. Havu, V. Havu, X. Ren, K. Reuter, and M. Scheffler, Comp. Phys. Comm. **180**, 2175 (2009).

[66] V. Havu, P. Havu, V. Blum, and M. Scheffler, J. Comput. Phys. **228**, 8367 (2009).

[67] H. J. Monkhorst and J. D. Pack, Phys. Rev. B **50**, 17953 (1976).

[68] G. Makov and M. C. Payne, Phys. Rev. B **51**, 4014 (1995).

[69] J. Neugebauer and M. Scheffler, Phys. Rev. B **46**, 16967 (1992).

[70] J. Klimeš, D. R. Bowler, and A. Michaelides, Phys. Rev. B **83**, 195131 (2011).

[71] G. Kresse and J. Hafner, Phys. Rev. B **47**, 558 (1993).

[72] G. Kresse and J. Furthmüller, Phys. Rev. B **54**, 11169 (1996).

[73] G. Román-Pérez and J. M. Soler, Phys. Rev. Lett. **103**, 096102 (2009).

[74] G. Kresse and D. Joubert, Phys. Rev. B **59**, 1758 (1999).

[75] M. Saeys, M. F. Reyniers, G. B. Marin, and M. Neurock, J. Phys. Chem. B **106**, 7489 (2002).

[76] A. Puzder, M. Dion, and D. C. Langreth, J. Chem. Phys. **124**, 164105 (2006).

[77] E. Ziambaras, J. Kleis, E. Schröder, and P. Hyldgaard, Phys. Rev. B **76**, 155425 (2007).

[78] I. Hamada, J. Chem. Phys. **133**, 214503 (2010).

[79] L. W. Bruch, R. D. Diehl, and J. A. Venables, Rev. Mod. Phys **79**, 1381 (2007).

[80] L. W. Bruch, M. W. Cole, and E. Zaremba, *Physical Adsorption: Forces and Phenomena* (Dover Publications, 2009).

[81] J. L. F. Da Silva, C. Stampfl, and M. Scheffler, Phys. Rev. B **72**, 075424 (2005).

[82] A. Ambrosetti and P. L. Silvestrelli, Phys. Rev. B **85**, 073101 (2012).

[83] O. A. Vydrov and T. Van Voorhis, Phys. Rev. A **81**, 062708 (2010).

[84] P. Haas, F. Tran, and P. Blaha, Phys. Rev. B **79**, 085104 (2009).

[85] C. T. Campbell and J. R. V. Sellers, J. Am. Chem. Soc. **134**, 18109 (2012).

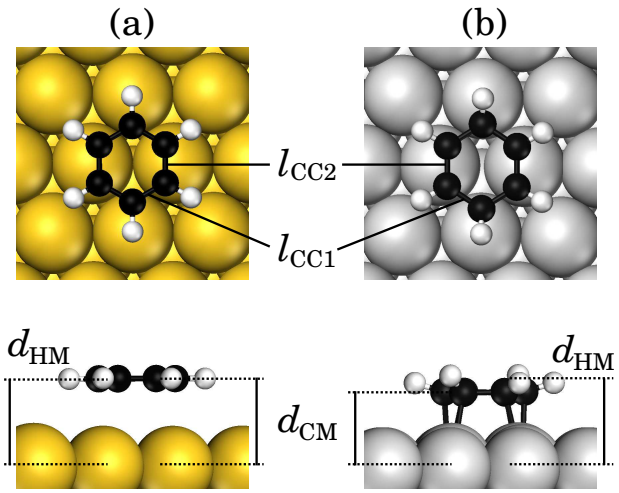

FIG. 1: Top and side views of a benzene molecule adsorbed at the bri30° site on the (111) surfaces of Cu, Ag, and Au (a) and Pd, Pt, Rh, and Ir (b). The average heights between carbon (hydrogen) and metal surface atoms, d_{CM} (d_{HM}), and the average C–C bond lengths within the adsorbed benzene molecule, l_{CC1} and l_{CC2}, are indicated. The d_{CM} (d_{HM}) height is defined as the perpendicular distance between the two xy parallel planes containing the average z coordinate of the C (H) atoms within the benzene molecule and the average z coordinate of the metal atoms in the topmost surface layer.

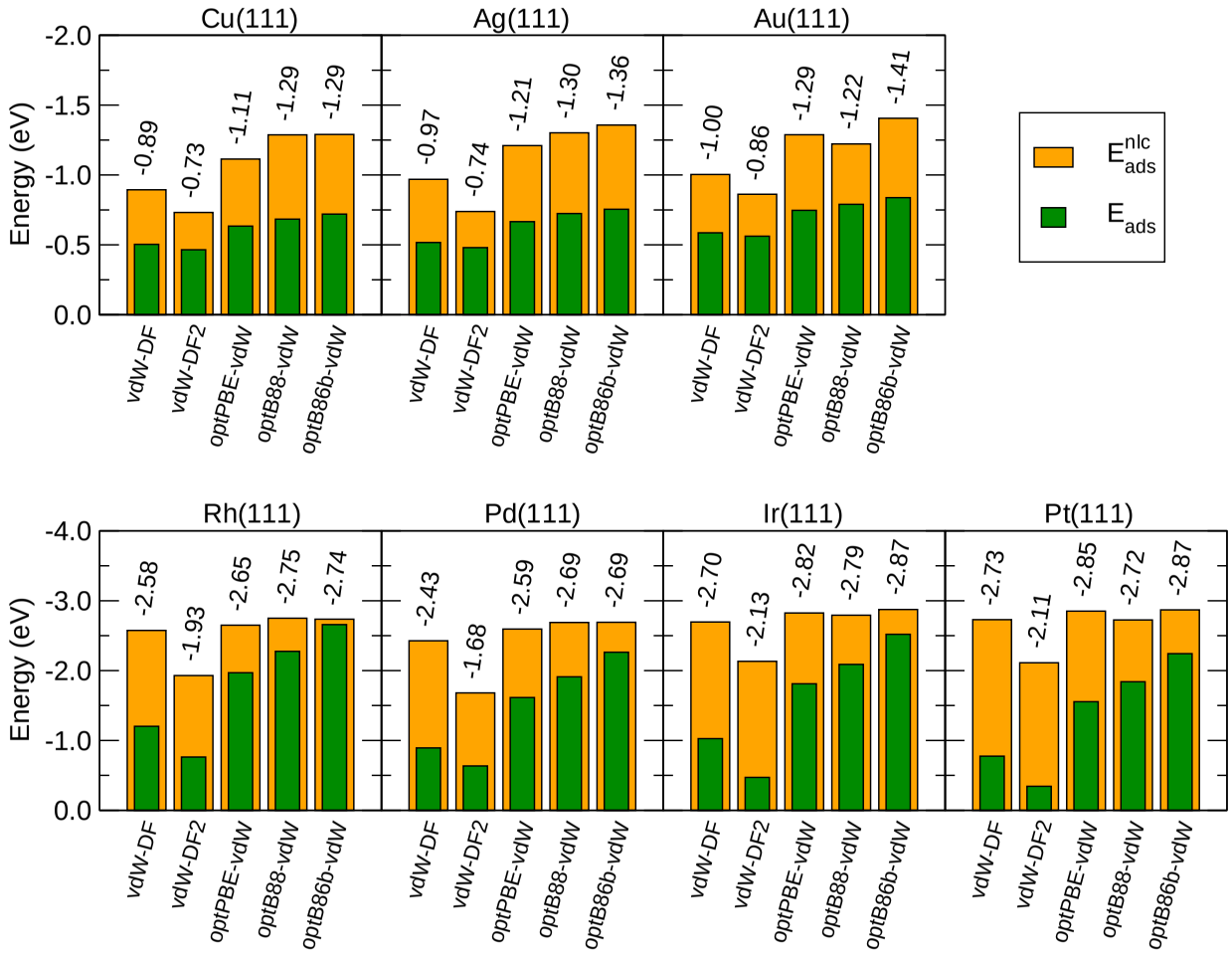

FIG. 2: Adsorption energies (thin centered green bars) and non-local correlation contribution to those (thick orange bars and associated numbers) of a benzene molecule adsorbed on the (111) surfaces of Cu, Ag, Au, Pd, Pt, Rh, and Ir. Five different density functionals are considered: vdW-DF, vdW-DF2, optPBE-vdW, optB88-vdW, and optB86b-vdW.

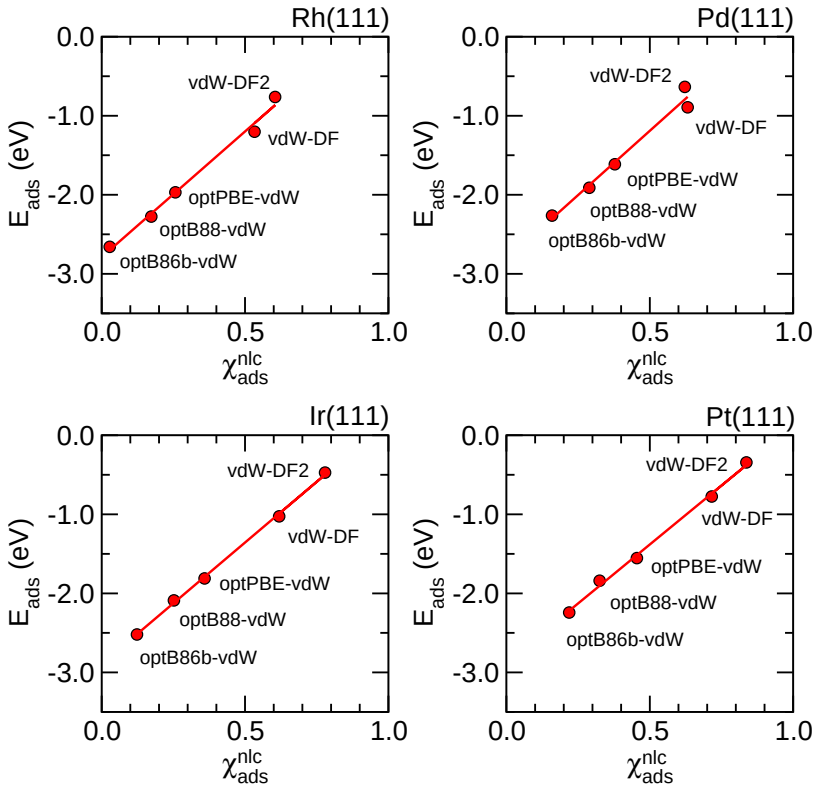

FIG. 3: Adsorption energy as a function of $\chi_{\rm ads}^{\rm nlc}$ (Eq. 3) for benzene on Rh, Pd, Ir, and Pt using vdW-DF, vdW-DF2, optPBE-vdW, optB88-vdW, and optB86b-vdW. The solid lines correspond to fitted linear regressions.

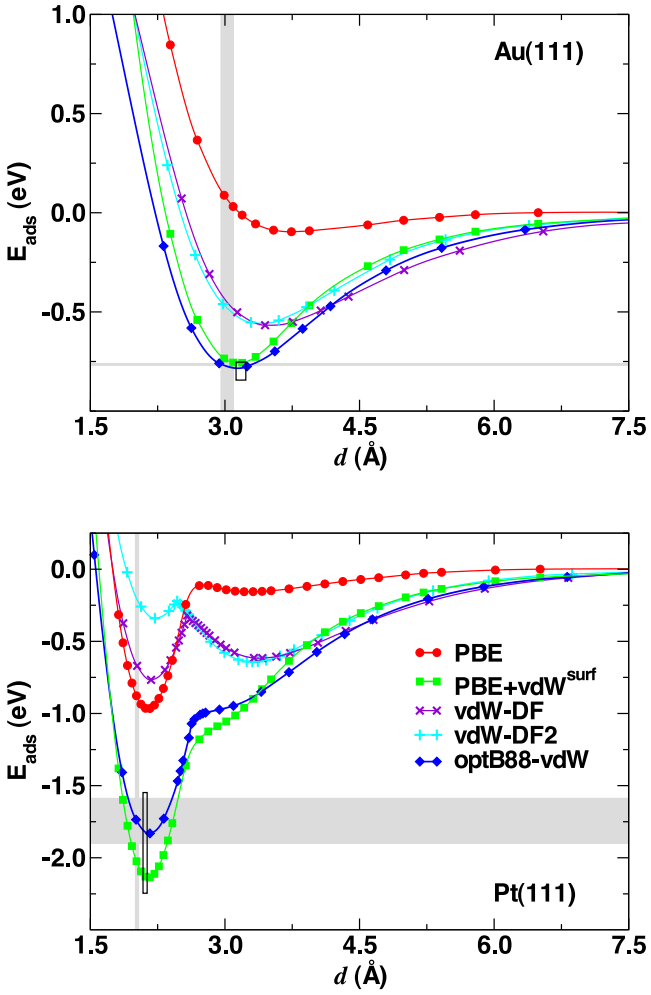

FIG. 4: Adsorption energy of benzene on Au(111) and Pt(111) as a function of the height d (see text). Five different methods are considered: PBE, PBE+vdW, PBE+vdW$^{\rm surf}$, vdW-DF, vdW-DF2, and optB88-vdW. The lines are merely a guide to the eye. Here, PBE+vdW$^{\rm surf}$ calculations are carried out using atomic ZORA for describing scalar relativistic effects. Our previous calculations in Refs. [18,38,39] employed scaled ZORA, leading to better agreement with experiments and to the appearance of a shallow physisorption precursor state for benzene on Pt. The grey bands indicate experimental binding distance (vertical) and adsorption energy (horizontal) ranges. The open black rectangles indicate the range of binding distances and adsorption energies from optPBE-vdW and optB86b-vdW as given in Tables III and IV: in the case of benzene adsorption on Pt, different optimized density functionals yield adsorption energy differences up to 0.7 eV. This situation is in contrast to the S22 database, for which all the optimized non-local functionals considered here essentially yield similar results.

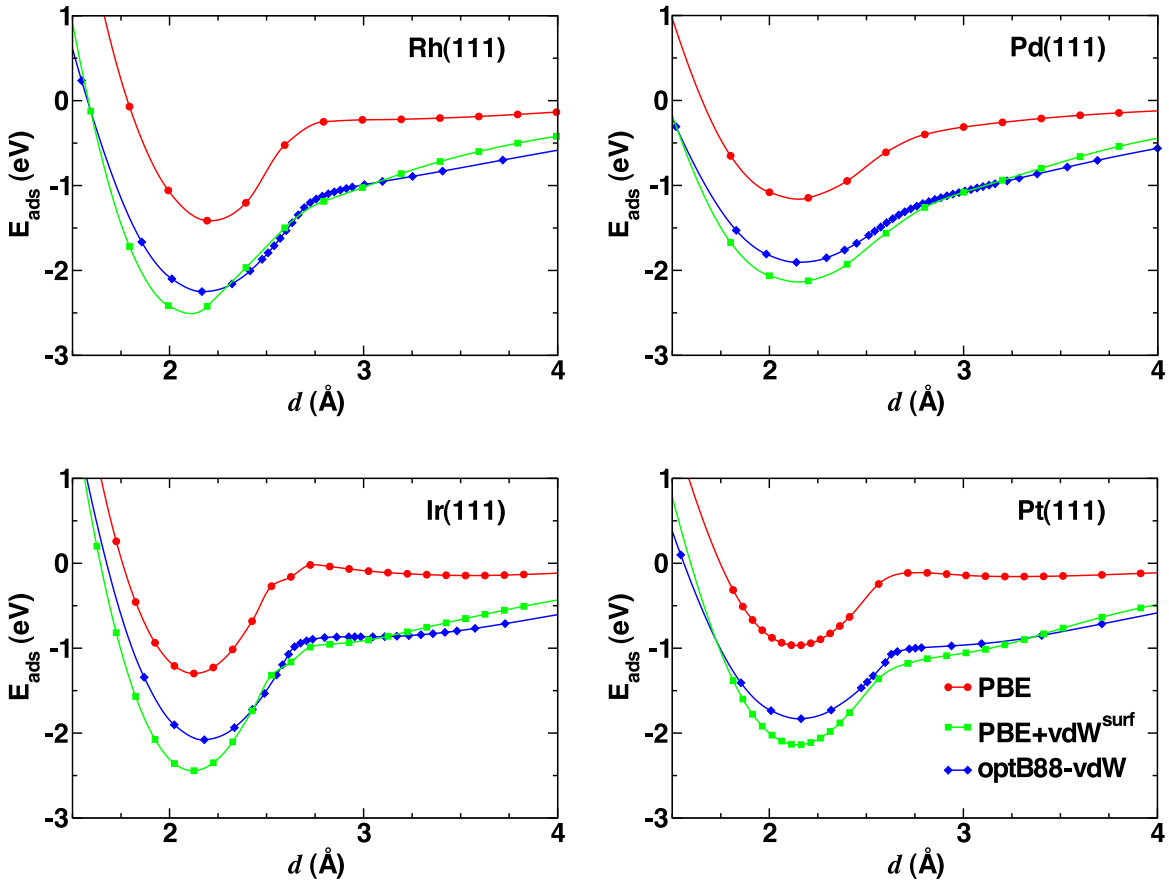

FIG. 5: Adsorption energy of benzene on Rh(111), Pd(111), Ir(111), and Pt(111) as a function of the height d (see text). Three different methods are considered: PBE, PBE+vdW$^{\rm surf}$, and optB88-vdW. The lines are merely a guide to the eye.

TABLE I: Adsorption energies in eV and equilibrium distances in Å as a function computational set-up for benzene adsorption on Au(111) and Pt(111) using PBE+vdW$^{\mathrm{surf}}$ (FHI-aims) and optB88-vdW (VASP).

	Au			Pt		
	E_{ads}	d_{CM}	d_{HM}	E_{ads}	d_{CM}	d_{HM}
	PBE+vdW$^{\mathrm{surf}}$					
Standard setup[a]	**−0.73**	**3.05**	**3.04**	**−2.14**	**2.08**	**2.51**
Tight tier3	−0.72	3.05	3.04	−2.15	2.08	2.51
8×8×1 **k**-point mesh	−0.75	3.05	3.04	−2.19	2.08	2.51
30 Å of vacuum	−0.72	3.05	3.04	−2.19	2.08	2.51
9 atomic layers slab	−0.74	3.05	3.04	−2.15	2.08	2.51
3 topmost atomic layers relaxed	−0.72	3.05	3.04	−2.14	2.09	2.52
	optB88-vdW					
Standard setup[b]	**−0.79**	**3.23**	**3.23**	**−1.84**	**2.12**	**2.53**
Cutoff energy of 1000 eV	−0.79	3.23	3.23	−1.83	2.12	2.53
6×6×1 **k**-point mesh	−0.78	3.23	3.23	−1.85	2.12	2.53
22 Å of vacuum	−0.77	3.23	3.23	−1.83	2.12	2.53
9 atomic layers slab	−0.78	3.23	3.23	−1.83	2.12	2.54
4 topmost atomic layers relaxed	−0.79	3.23	3.23	−1.84	2.12	2.54

[a]Tight tier2; 6×6×1 **k**-point mesh; 20 Å of vacuum; 6 atomic layers slab; 2 topmost atomic layers relaxed.
[b]Cutoff energy of 500 eV; 4×4×1 **k**-point mesh; 12 Å of vacuum; 6 atomic layers slab; 3 topmost atomic layers relaxed.

TABLE II: Optimized lattice constants in Å of bulk metals for different vdW-inclusive methods considered in the present work. In addition, PBE values are shown. The values are compared to the experimental values corrected for the zero-point anharmonic expansion,[84] non-corrected values are shown in parenthesis.

Method	Cu	Ag	Au	Rh	Pd	Ir	Pt
PBE	3.631	4.149	4.159	3.830	3.943	3.871	3.971
PBE+vdW	3.543	4.071	4.116	3.773	3.913	3.844	3.939
PBE+vdW^{surf}	3.572	4.007	4.163	3.765	3.949	3.873	3.979
vdW-DF	3.699	4.260	4.241	3.877	4.006	3.929	4.030
vdW-DF2	3.742	4.329	4.333	3.939	4.075	3.992	4.107
optPBE-vdW	3.646	4.181	4.178	3.838	3.951	3.898	3.989
optB88-vdW	3.623	4.147	4.158	3.826	3.933	3.891	3.978
optB86b-vdW	3.596	4.109	4.119	3.800	3.902	3.866	3.948
Experiment	3.596	4.062	4.062	3.793	3.876	3.831	3.913
	(3.603)	(4.069)	(4.065)	(3.798)	(3.881)	(3.835)	(3.916)

TABLE III: Calculated adsorption energies in eV for benzene on different metal surfaces at the bri30° site. Available experimental data is also provided for comparison. Experimental data for coinage metals has been determined from TPD measurements and it has been corrected by the method developed by Campbell and Seller[85] to reliably predict the pre-exponential factor in the Redhead formula as described in Ref. [39].

Method	Cu	Ag	Au	Rh	Pd	Ir	Pt
PBE	−0.08	−0.08	−0.08	−1.44	−1.16	−1.26	−1.00
PBE+vdW	−1.02	−0.82	−0.80	−2.73	−2.02	−2.35	−1.98
PBE+vdW^{surf}	−0.79	−0.73	−0.73	−2.46	−2.13	−2.40	−2.14
vdW-DF	−0.50	−0.52	−0.59	−1.20	−0.89	−1.03	−0.77
vdW-DF2	−0.47	−0.48	−0.56	−0.76	−0.64	−0.47	−0.34
optPBE-vdW	−0.63	−0.67	−0.75	−1.97	−1.61	−1.81	−1.55
optB88-vdW	−0.68	−0.72	−0.79	−2.27	−1.91	−2.09	−1.84
optB86b-vdW	−0.72	−0.76	−0.84	−2.66	−2.26	−2.52	−2.24
Experiment	−0.71[a]	−0.69[b]	−0.76[c]				−1.91–1.57[d]

[a]Refs. [57,85]
[b]Refs. [54,85].
[c]Refs. [59,85].
[d]Microcalorimetry measurements from Ref. [60].

TABLE IV: Calculated d_{CM}, d_{HM}, l_{CC1}, and l_{CC2} in Å as defined in Fig. 1. For coinage metal surfaces l_{CC1} has the same value as l_{CC2}.

	Method	Cu	Ag	Au	Rh	Pd	Ir	Pt
d_{CM}	PBE	3.74	3.69	3.62[a]	2.14	2.12	2.15	2.10[b]
	PBE+vdW	3.04	3.14	3.21[a]	2.14	2.12	2.14	2.11[b]
	PBE+vdW$^{\mathrm{surf}}$	2.79	2.96	3.05[a]	2.12	2.10	2.13	2.08[b]
	vdW-DF	4.14	3.95	3.44[a]	2.19	2.21	219	2.16[b]
	vdW-DF2	3.38	3.40	3.29[a]	2.25	2.40	2.23	2.20[b]
	optPBE-vdW	3.28	3.29	3.22[a]	2.16	2.15	2.16	2.12[b]
	optB88-vdW	3.08	3.12	3.23[a]	2.14	2.13	2.15	2.12[b]
	optB86b-vdW	3.12	3.10	3.12[a]	2.13	2.11	2.13	2.10[b]
d_{HM}	PBE	3.74	3.70	3.62	2.55	2.47	2.60	2.54
	PBE+vdW	3.06	3.15	3.20	2.53	2.47	2.59	2.53
	PBE+vdW$^{\mathrm{surf}}$	2.79	2.95	3.04	2.51	2.46	2.57	2.51
	vdW-DF	4.13	3.95	3.42	2.58	2.53	2.64	2.57
	vdW-DF2	3.37	3.39	3.27	2.61	2.60	2.65	2.65
	optPBE-vdW	3.27	3.28	3.22	2.56	2.49	2.59	2.54
	optB88-vdW	3.06	3.12	3.23	2.53	2.46	2.59	2.53
	optB86b-vdW	3.11	3.10	3.12	2.53	2.46	2.58	2.52
l_{CC1} (l_{CC2})	PBE	1.40	1.40	1.40	1.47 (1.44)	1.45 (1.43)	1.48 (1.44)	1.47 (1.43)
	PBE+vdW	1.40	1.40	1.40	1.47 (1.44)	1.45 (1.43)	1.48 (1.44)	1.48 (1.44)
	PBE+vdW$^{\mathrm{surf}}$	1.40	1.40	1.40	1.47 (1.43)	1.45 (1.43)	1.48 (1.44)	1.48 (1.43)
	vdW-DF	1.40	1.40	1.40	1.47 (1.44)	1.45 (1.43)	1.48 (1.44)	1.48 (1.44)
	vdW-DF2	1.40	1.40	1.40	1.46 (1.43)	1.43 (1.42)	1.48 (1.43)	1.47 (1.43)
	optPBE-vdW	1.40	1.40	1.40	1.47 (1.43)	1.45 (1.43)	1.48 (1.44)	1.48 (1.44)
	optB88-vdW	1.40	1.40	1.40	1.46 (1.43)	1.45 (1.43)	1.48 (1.43)	1.47 (1.43)
	optB86b-vdW	1.40	1.40	1.40	1.46 (1.43)	1.45 (1.43)	1.48 (1.44)	1.48 (1.44)

[a]To be compared with deduced data from work function and pentacene adsorption experiments,[17,62,63] 3.03±0.08 Å.

[b]To be compared with LEED measurements,[55] 2.02±0.02 Å.

TABLE V: C_3 coefficients in eVÅ^3 (obtained from Eq. 4) for benzene on Au and Pt using PBE+vdW$^{\rm surf}$, vdW-DF, vdW-DF2, and optB88-vdW.

Method	Au	Pt
PBE+vdW$^{\rm surf}$	9.16±0.08	9.77±0.13
vdW-DF	8.94±0.18	9.76±0.20
vdW-DF2	4.86±0.08	5.64±0.07
optB88-vdW	8.66±0.18	9.14±0.22